2024 IEEE International Conference on Robotics and Automation (ICRA 2024)
May 13-17, 2024. Yokohama, Japan

HyperLeg: Biomechanics-Inspired High-DOF Leg and Toe Mechanism for Highly Dynamic Motions

Do-Yun Kim, Seong-Ho Yun, Joong-Kyung Lee, Jongjun Yoon, Dongyun Nam, Chan-Young Maeng, and Yong-Jae Kim

Abstract— **A human foot with high degrees of freedom (DOF) that has multi-DOF toe joints and a two-DOF ankle provides multiple benefits, such as increased stride length and walking speed, impact mitigation, and enhanced balancing. However, creating such mechanisms for legged robots has been challenging due to increased complexity, heavy weight, and vulnerability to impact. In this paper, a novel leg and toe mechanism inspired by human biomechanics, featuring a one-DOF knee joint, two-DOF ankle joint, and one-DOF toe joint, is developed. All actuators are located at the proximal part of the thigh frame to minimize the distal mass. High payload timing belts and unique linkage mechanisms are utilized in the transmission to achieve high backdrivability and high joint stiffness. Actuation torques are intentionally coupled inspired by human anatomy, enduring the high propulsive force to the ground for dynamic movements, such as jumping. The implemented leg and toe mechanisms weigh 8.16 kg, and the height from the ground to the hip center is 786 mm. The proposed mechanism has been proven to be effective through force test and distance jump experiments.**

I. Introduction

The human foot was designed to absorb impacts and adapt to various spatial configurations on different ground surfaces [1]. Human toes significantly contribute to balance and propulsion. During walking, the highest pressure is exerted on the toes compared to all soles [2]. In particular, the big toe helps maintain static balance in the single-leg posture and the ability to adjust the walking direction. [3]. Therefore, humans can perform highly dynamic motions such as jumping, running, and sprinting, as well as delicate and acrobatic motion such as ballet, dancing, and gymnastics. Despite the multiple functions of the feet and toes, most legged robots do not exploit these advantages. Biped robots have evolved from conventional manipulator technologies [4][5][6] and have exhibited outstanding performance using precise motion control in bent-knee poses to adapt to the ground and avoid impact from the ground. They have flat and blocky feet connected to a two-DOF ankle joint and are suitable for walking smoothly without considerable impact on the ground.

*Research supported by by Future Mobility Project of WIRobotics Co.

Yong-Jae Kim, is with Korea University of Technology and Education (KOREATECH), Cheonan-City, Rep. of Korea (corresponding author to provide phone: +82-41-560-1424; fax: +82-41-564-3261; e-mail: yongjae@koreatech.ac.kr).

Do-Yun Kim, Seong-Ho Yun, Joong-Kyung Lee, Jongjun Yoon, Dongyun Nam, and Chan-Young Maeng are with Korea University of Technology and Education (KOREATECH), Cheonan-City, Rep. of Korea (e-mail: ehdbs9@koreatech.ac.kr, dnstjdgh@koreatech.ac.kr, jkyung96@koreatech.ac.kr, bluejjx@koreatech.ac.kr, ndy0422@koreatech.ac.kr, and aodrnrj@koreatech.ac.kr).

Fig. 1. Developed high-DOF leg and toe mechanism HyperLeg.

However, they are unsuitable for rough or unpredictable terrains or dynamic high-impact walking and running. Efforts have been made to achieve a high level of backdrivability by utilizing tendons and ball screws [7][8], absorbing impact using a series of elastic actuators [9], or realizing stable walking on uneven terrain with sensors [10][11]; however, their complicated and heavy ankle and foot mechanisms hinders agile movement and decreasing robustness against impact.

Many quadrupedal robots using a quasi-direct drive (QDD) with extremely light limbs have achieved considerable success with advances in optimization and machine-learning techniques [12][13]. These robots have a non-collocated structure in which the actuators are placed at the proximal frame and not at the corresponding joints. Recently, many research groups have attempted to develop biped robots with these properties [14][15][16]. Moreover, non-collocated leg mechanisms with a carefully coupled actuation structure inspired by biomechanics demonstrate high energy efficiency and walking performance [17][18][19]. Implementing a non-collocated high-DOF foot and ankle mechanism is challenging, particularly when it is lightweight and endures impacts. Thus, most of these biped robots have pointed or small rigid feet with one-DOF ankles, neglecting the advantages of high-DOF ankles and toes. Various toe mechanisms have been proposed for biped robots [20][21][22][23]. These toe mechanisms have been proven to increase the walking stride length and enable a humanlike walking style with a stretched knee pose. Passive toe

mechanisms [20][21] are relatively simple and light, and provide stable contact with the ground, especially during the toe-off phase; however, delivering propulsive force and active balancing through the toe is challenging. Active toes [22] or variable-stiffness toes [23] can help in balance and propulsion; however, they can be heavier than human toes, vulnerable to ground impact, and unsuitable for dynamic motion.

Unlike the small feet of recent non-collocated biped robots, the human foot is sufficiently large compared to other limbs, and effectively delivers force to the toes because of the connection of the Achilles tendon, the calcaneus bone, and plantar fascia with intrinsic foot muscles. It can absorb shock and distribute the load to the soles and toes. To obtain human-like capabilities in a robotic mechanism, the foot mechanism should be light, robust, backdrivable with high DOF and low inertia. As shown in Fig.1, this paper presents a new leg and foot mechanism called HyperLeg, inspired by human biomechanics. It includes a one-DOF knee joint, a two-DOF ankle joint, and a one-DOF toe joint. All the actuators for these joints were placed at the proximal part of the thigh frame to minimize the distal mass and increase foot robustness. To achieve backdrivability and high joint stiffness, high-payload timing belts and specially designed linkage mechanisms were used for the transmission. This transmission mechanism intentionally couples actuators and joints inspired by the human anatomy, enduring a high propulsive force on the ground for dynamic movements such as jumping. The unique serial connection of the two Watt 6-bar linkages affords a wide range of ankle and toe motions, similar to those of humans.

The remainder of this paper is organized as follows: Section II explains the design concept of HyperLeg and demonstrates its properties and effectiveness using a kinematic; Section III describes the detailed design and implementation of the study; Section IV reports the experimental results; and Section IV concludes the paper.

II. Design Concept

A. Human Legs and Robotics Legs

Fig. 2 illustrates the human foot and simplified planar models of several robotic leg mechanisms with feet, where the blue circles denote active joints or actuators and the gray circles denote passive pulleys or joints. Fig 2(a) and (b) illustrates the interconnections of the muscle, tendons, and fascia in the human foot. These components form an effective structure that transmits muscle force to the ground. As shown in Fig. 2(a) with dotted red lines, the calcaneal, tarsal, metatarsal bones, and plantar fascia wrapping around the head of the metatarsal bone form a triangular structure named windlass mechanism [1]. This makes the foot rigid to effectively transfer the propulsion force especially when the walking phase from mid-stance to toe-off [1]. Fig. 2(b) shows two joints of the human foot: the ankle joint for dorsiflexion and plantar flexion, and the subtalar joint for pronation and supination. The ankle joint is located between the talus, tibia, and fibular bones, permitting dorsiflexion and plantar flexion. The subtalar joint is located between the talus

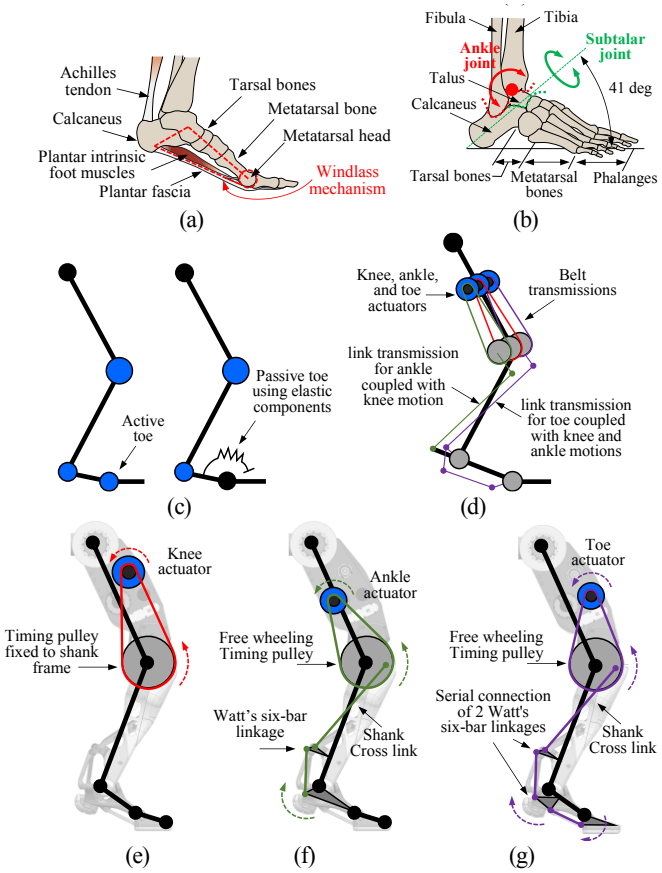

Fig. 2 (a)-(b) Closed up views of the human foot with the windlass mechanism and joints in the ankle. (c) Simplified planar models of legs with toes (blue circles: actuators). (d) Proposed concept of HyperLeg (gray circles: passive or fixed pulleys). (e)-(g) Configurations of transmissions for knee, ankle, and toe actuations.

and two tarsal bones. Remarkably, the axis of the subtalar joint was tilted backward by approximately 41 deg to pass through the heel contact point of the calcaneus [2]. This joint configuration helps stabilize heel contact because the heel maintains the same contact position regardless of the subtalar joint angle [24]. Additionally, the combined mass of the human shank and foot is approximately 5 kg [25], which is difficult to achieve using collocated actuation.

Biped robots can have a two-DOF ankle joint, similar to that of human ankles. Fig. 2(c) shows the concepts of active and passive toe mechanisms, where the models were simplified to one-degree-of-freedom (DOF) ankles for ease of explanation. Active toes [22] can change gait and enhance stability by minutely adjusting the center of pressure (COP) of the toe, especially during the toe-off phase. However, an active toe mechanism with a collocated structure makes the foot heavy and vulnerable to impact. Passive toes [20][21] or variable-compliance toes [23] can be good tradeoffs to make the foot lightweight; however, their contribution to balancing and propulsion is limited, and the effect may be similar to that of a properly designed curved sole mechanism without toes.

Figs. 2(e)–(g) illustrate the proposed HyperLeg concept. Unlike other toe mechanisms, all the toe and ankle actuators are located in the thigh frame. Thus, a light weight and

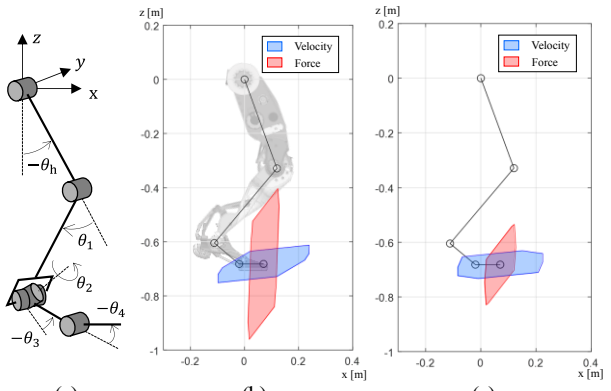

(a) (b) (c)

Fig. 3. (a) Joint configuration and coordinate system of HyperLeg. (b) Velocity and force polygons of HyperLeg. (c) Velocity and force polygons using collocated actuation.

robustness can be achieved without losing degrees of freedom or high force. To implement such a non-collocated leg, an efficient transmission mechanism with a high payload and stiffness, low inertia and friction, and large-range motion is required. The red, green, and purple lines represent the transmission belts and linkages for knee, ankle, and toe actuation, respectively. For the actual implementation of the two-DOF ankle joints, two sets of mechanisms, as shown in Fig. 2(f), were used in parallel, as explained in Section III and Fig. 5. The dotted arrows in Figs. 2(e), (f), and (g) show the torque directions of the joints generated by the actuators. All actuator torques acted cooperatively in the direction of pushing the ground: knee extension, ankle plantar flexion, and toe plantar flexion. To exploit this coupling advantage and deliver the force effectively, as shown in Figs. 2(f) and (g), the linkage configurations were carefully designed. For instance, the shank crosslink connects the front point of the pulley on the knee joint and the rear point of the ankle to receive a tensile force and prevent buckling when pushing the ground. Generally, linkage mechanisms can achieve high stiffness and robustness because of their relatively simple and sturdy structures; however, they have a limited range of motion. To overcome this problem, as shown in Fig. 2(f), a Watt-type six-bar linkage mechanism was used in a series of shank-crossed links; thus, a wide human-like range of motion was achieved. To further exploit the coupling effect of human toes, as shown in Fig. 2(g), the shank crosslink was connected to two Watt-type six-bar linkages in series. Therefore, the toe actuator can deliver a high torque to the toe joint without increasing the foot mass and contribute to knee extension and ankle plantar flexion.

B. Force-Torque Relationship and Cooperative Actuation

In HyperLeg, four actuators are located in the thigh frame and intentionally coupled with the one-DOF knee, two-DOF ankle, and one-DOF toe joints to exert the maximum force on the ground during dynamic motion. Sim et al. named this design principle as cooperative actuation (CA) [14]. The CA effect of the HyperLeg can be identified by evaluating the relationship between the actuator and joint torques, as well as that between the joint torques and foot force. Fig. 3(a) shows the joint configuration of the proposed leg mechanism, where θ_h, θ_1, θ_2, θ_3, and θ_4 denote the hip pitch, knee pitch, ankle pitch, ankle roll, and toe pitch angles, respectively. Because this paper focuses on knee, ankle, and toe motions, $\theta = [\theta_1, \theta_2, \theta_3, \theta_4]^T$ will be mainly considered. From the connections between the actuators and joints shown in Figs. 2(e), (f), and (g), the forward kinematics f_a, Jacobian J_a, and torque relationship between the actuators and joints can be obtained as follows:

$$\theta = f_a(\phi), \dot{\theta} = J_a \dot{\phi}, \text{ and } \tau_{jt} = J_a^{-T} \tau_a \quad (1)$$

where ϕ denotes the 4×1 vectors representing the angles of the knee, left ankle, right ankle, and toe actuators, respectively, and τ_a and τ_{jt} denote the torque vectors of the actuator and joint, respectively. The left and right ankle actuators were connected to the left and right sides of the heel in parallel via belts and linkages, as shown in Figs. 4(b) and (e), respectively, which are omitted in Fig. 2(f). This kinematic relationship is nonlinear and its derivation is explained in Subsection III.B. As an example, if the leg is in a knee-bent pose pressing the ground with the toe, i.e., $\theta_h = -20$ and $\theta = [60, 0, 0, -40]^T$ deg as shown in Figs. 3(b), the torque relationship of (1) becomes

$$\tau_{jt} = \begin{bmatrix} -31.11 & -31.11 & -31.11 & -31.11 \\ 0 & 26.69 & 26.69 & 19.23 \\ 0 & 16.51 & -16.51 & 0 \\ 0 & 0 & 0 & 21.27 \end{bmatrix} \tau_a \quad (2)$$

As noted by the fact that the first row has non-zero negative values, all four actuators cooperatively produce knee joint torque in the extension direction. The second and fourth rows of the ankle pitch and toe joints exhibited the same positive values, indicating that when all actuators produced joint torques in the direction of knee extension, they cooperatively produced ankle and toe plantar flexion torques, all of which helped support the body weight and propulsion. As explained in [14], the ankle roll joint corresponding to the third row of (2) can also be interpreted as a CA using a parallel link connection.

The kinematic relationship f_{jt}, Jacobian J_{jt}, and force-torque relationship between the joints and toe position are as follows:

$$p_{toe} = f_{jt}(\theta), \dot{p}_{toe} = J_{jt}\dot{\theta}, \text{ and } f_{toe} = J_{jt}^{+T} \tau_{jt} \quad (3)$$

where $p_{toe} = [x_t, y_t, z_t]$ denotes the position of the center of the toe frame. f_{toe} is the force on the toe, and the operator $(\cdot)^{+T}$ represents the transpose of the pseudo-inverse matrix. By combining (1) and (3), the velocity and force relationship between the actuators and toe can be obtained as follows:

$$\dot{p}_{toe} = J_{jt} J_a \dot{\phi} \quad (4)$$

$$f_{toe} = J_{jt}^{+T} J_a^{-T} \tau_a \quad (5)$$

Figs. 3(b) and (c) illustrate the force and velocity polygons that the robot can produce, respectively, where (4) and (5) are extended to include the hip joint motions. For the calculation, the actual values of the peak torques and speeds of the knee, ankle, and toe motors listed in Table I were used, and the speed and torque of the hip-pitch actuator were set as 910°/s and 250 Nm, respectively. Fig. 3(b) shows the results of the CA of HyperLeg, where the matrix J_a^{-T} in (2) was used. Fig.

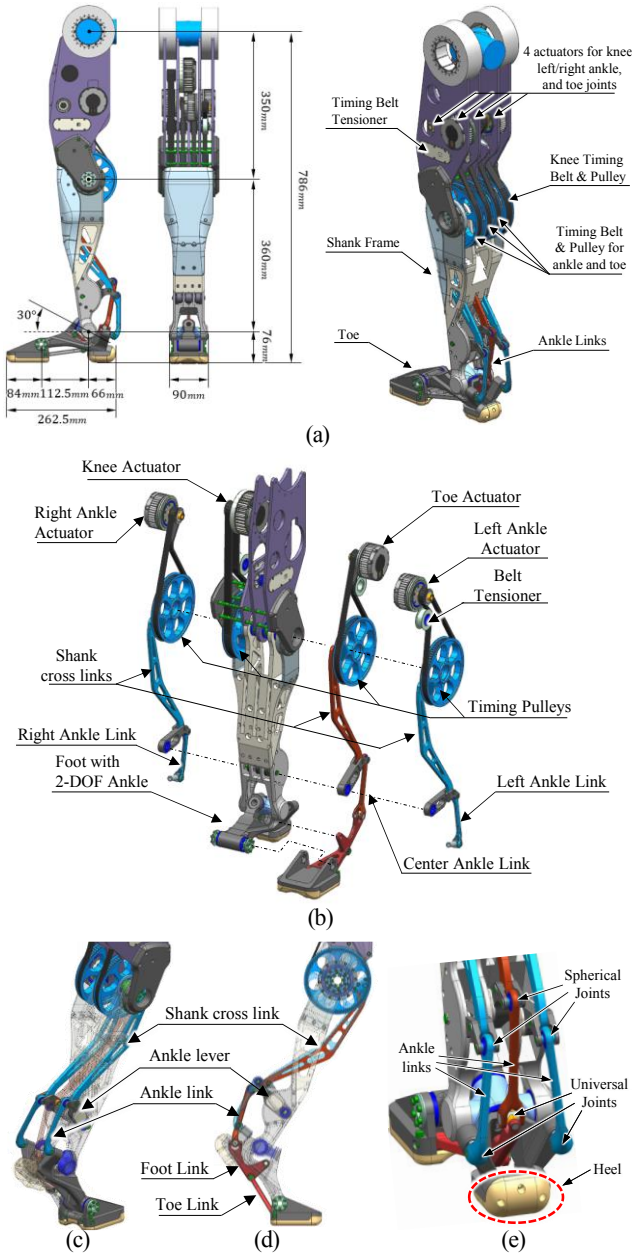

Fig. 4. Mechanical design of the HyperLeg. (a),(b) Detailed design and exploded view of the proposed HyperLeg. (c), (d), and (e) Design of the linkage mechanisms for the ankle and toe actuations

3(c) shows the results of the collocated actuation, where J_a^{-T} has only diagonal terms. The collocated actuation shown in Fig. 3(c) has a small force polygon. It can also have practical implementation problems, such as a large distal mass, complicated ankle and foot mechanisms, and impact vulnerability. Owing to the CA, the HyperLeg exerts a significantly large force, particularly in the direction of pushing the ground. However, the proposed CA may degrade the performance of other motions or applications. For example, it reduces the torque in the direction of ankle dorsiflexion because it is in the opposite direction to pushing the ground. In addition, the redundancy caused by the addition of toe DOF may make control and balance difficult.

Table I. Mechanical Specifications

Weight [kg]	**Total**	8.16			
	Thigh	**Shank**	**Ankle**	**Foot**	**Toe**
	3.94	2.98	0.13	0.68	0.43
Items	**Knee**	**Ankle pitch**	**Ankle roll**	**Toe**	
Range of motion [deg]	0~150	-56~60	-30~30	-65~10	
Equivalent reduction ratio*	31.11 : 1	26.69 : 1	16.51 : 1	31.93 : 1	
Motors	RI70	RI60	RI60	RI60	
Max speed [deg/s]	602.7	785.6	1270.4	656.8	
Rated torque without CA [Nm]	26.32	13.69	8.47	16.38	
Max torque without CA [Nm]	75.04	39.16	24.21	46.84	
Max torque with CA [Nm]	212.0	111.7	48.44	46.84	
Reduction ratio from motors to pulleys	Planetary Gear (7:1) × Timing Pulley (4.44:1)				
Motor specification	RI70, T-Motor Co. Peak torque: 2.68 Nm Cont. torque: 0.94 Nm No load speed: 18,750 deg/s		RI60, T-Motor Co. Peak torque: 1.63 Nm Cont. torque: 0.57 Nm No load speed: 20,970 deg/s		

* Reduction ratios from motors at a standing pose as shown in Fig. 4(a)

III. Detailed Design and Implementation

A. Mechanical Design

The proposed leg height was 786 mm. The distance between the tip of the toe and the end of the heel was 262.5 mm, and the transverse length of the toe was 90 mm. To effectively absorb the impact from the heel, the axis of the ankle-roll joint was designed to pass through the heel at an angle of 30° from the ground, similar to that in humans. The knee, left ankle, right ankle, and toe actuators are located inside the thigh frame, as shown in Figs. 4(a) and (b). The output from each actuator was connected to the corresponding timing pulley at the knee joint through a timing belt. As shown in Fig. 4(b), a timing pulley was attached to the shank frame to actuate the knee joint, and the other pulleys were connected to the shank crosslinks for ankle and toe actuation. Figs. 4(c) and (d) illustrate the linkage mechanisms for the ankle and toe. The ankle levers, ankle links, shank cross links, and timing pulleys at the knee joint form Watt-type six-bar mechanisms, which enable a wide range of motions of the ankle and toe joints, similar to humans. In particular, as shown in Fig. 4(d), the linkage configuration was carefully determined to ensure that all links were under tension when the toe exerted a large force against the ground to prevent the damage or buckling, even under severe impacts. In addition, each link length was determined to ensure a wide range of motion for performing various motions and not to work in the singular region. As shown in Fig. 4(e), both ends of the ankle links were connected to other links or frames via spherical and universal joints to allow three-dimensional motion, as presented in the authors' previous study on a two-DOF ankle mechanism [26].

Table I summarizes the specifications of HyperLeg. The total weight of the mechanism is 8.16 kg. The thigh with actuators, the shank with the ankle joint, and the foot with the toe had masses of 3.94, 3.11, and 1.11 kg, respectively. The mass of the parts below the knee was 4.22 kg, which is much

Fig. 5. Various Ankle and toe joint motions.

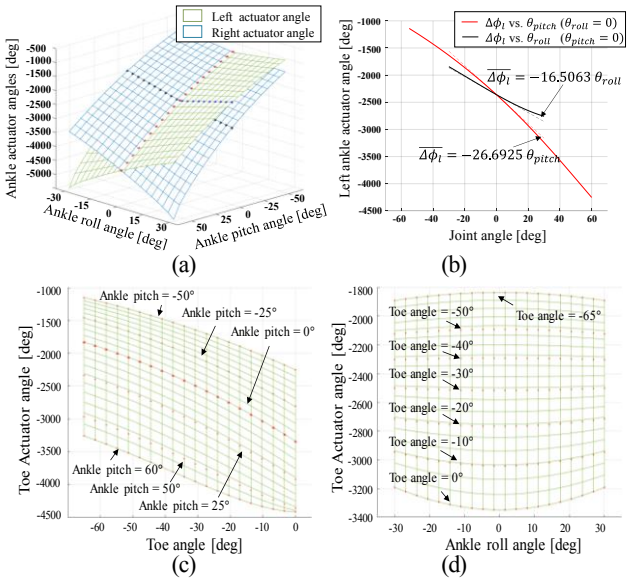

Fig. 6. (a), (b) Relationship between the ankle actuators and ankle joints. (c), (d) Relationship between the toe actuators and toe and ankle joints.

lighter than most human-sized collocated biped robots and comparable to that of an adult male at 5 kg [25]. Each motor has a one-stage planetary gear developed from scratch by machining and nitriding the steel gears. The reduction ratio of the planetary gear is 7:1. The timing belt and pulley produced an additional reduction ratio of 4.44:1. To prevent damage to the reducers by the propagation of impact from the ground, the motor rotors and gears were carefully designed to have low inertia. As indicated by the speed and torque specifications of the joints, CA increased the peak torque of the knee and ankle joints. For instance, although the knee actuator alone produces a peak torque of 75.04 Nm, with the help of the CA, the peak torque of the knee joint can be increased to 212 Nm.

The materials of the components were selected to make the legs lighter and more robust. For simplicity, the thigh frame was composed of four AL6061-T6 plates for simple construction. For weight reduction, a shank frame was built using 3D-printed acrylonitrile-butadiene-styrene (ABS) parts. The foot and toe frames and links were made of AL6061-T6 material to ensure robustness against impact. Polyurethane was used as the material for the toe and heel pads. The toe pad was designed to be sufficiently large to achieve sufficient friction, particularly at the toe-off moment of walking. The heel pad is designed to be spherical to ensure stable contact with the ground in the heel-contact stance. Fig. 5 shows the range of motion of the ankle and toe.

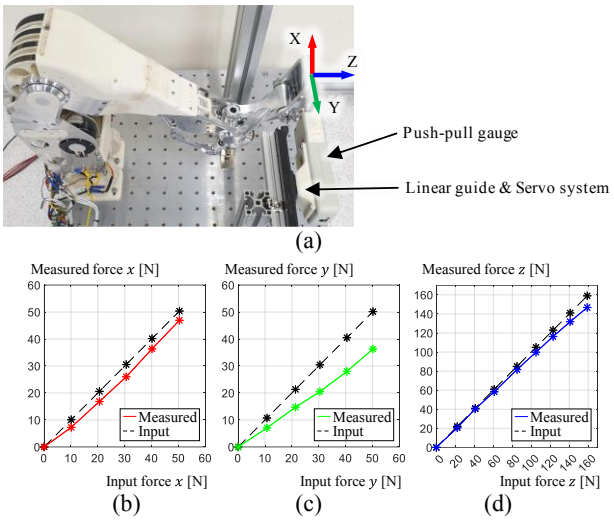

Fig. 7. Toe force test. (a) Experimental setup. (b), (c), and (d) Measured force using motor current in the direction of x, y, and z, respectively.

B. Kinematics

Obtaining inverse kinematics is convenient for mechanisms with coupled and parallel structures, such as HyperLeg. The inverse kinematics between the actuators and joints is the inverse function of (1), where the input is the joint angle and the output is the actuator angle. The inverse kinematics can be obtained similar to [26], and the forward kinematics and Jacobian were calculated numerically and iteratively using the obtained inverse kinematics. Figs. 6(a) and (b) illustrate the symmetrical relationship between the pitch and roll angles of the ankle joint and the left and right ankle actuator angles. As shown in Fig. 6(b), an approximately linear relationship is exhibited without significant distortions over the entire range of motion. Fig. 6(c) shows the relationship between the toe actuator and toe joint, which is also related to the ankle pitch angle. Fig. 6(d) shows that the ankle roll motion slightly affects the relationship between the toe joint motion and toe actuator motion. Although these relationships are nonlinear and coupled, motion planning and control can be performed appropriately because the control algorithms are based on the exact forward and backward kinematics and dynamics. In addition, because the nonlinear reduction ratios remain within the appropriate bounds, the leg can exert force and speed over the entire range of motion without distortion or singularity.

IV. Experimental Validation

A. Toe Force Test

To verify the force fidelity of the proposed leg mechanism, the actual force applied to the toe frame and estimated force calculated from the motor current were compared. As shown in Fig. 7(a), force was applied to the center of the toe frame in three directions using a linear guide, and the applied force was measured using a push-pull gauge (DS2-500N, YILIDA Co.). Figs. 7(b), (c), and (d) show the estimated forces calculated from the motor current using (5), which verify that the proposed leg mechanism is possible to detect external forces without force-torque sensors owing to the low friction of the transmission and accurate kinematic modeling. This error is thought to have occurred because of the remaining friction at the timing belt and bushings of the linkage joints, which can

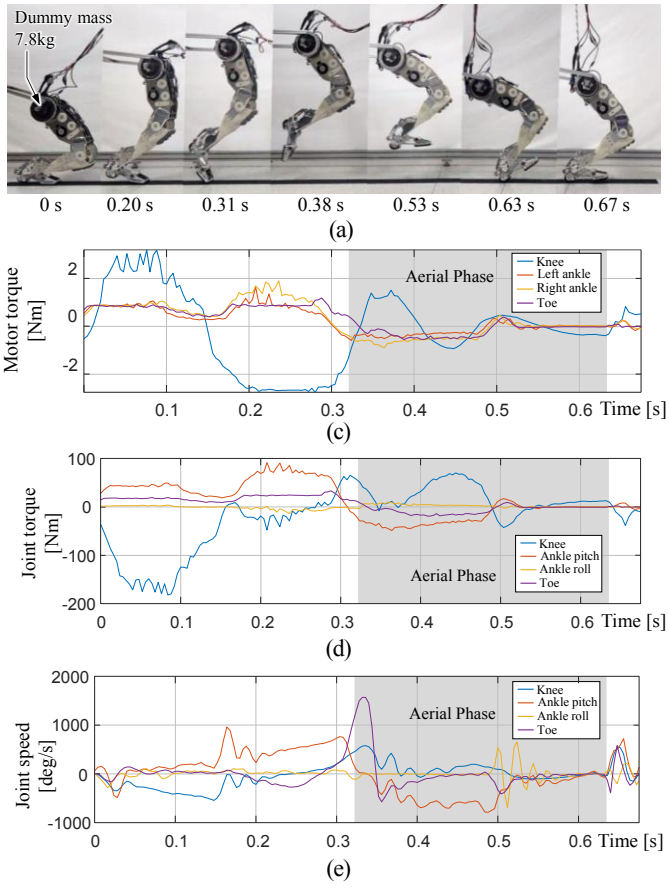

Fig. 8. Distance jumping test. (a) Snapshot of distance jumping. (b) Jumping pose captured using a motion capture system and GRF data. (c), (d), and (e) Motor torque, joint torque, and joint speed.

be improved by friction compensation. The maximum errors at the highest force were 4.56, 13.84, and 12.22 N in the x, y, and z directions, respectively.

B. Distance Jump Test

Distance jump experiments were conducted to prove that the proposed leg is suitable for dynamic and coordinated motion. A dummy mass of 7.8 kg was attached to the hip position, considering the mass of the three hip actuators and the upper body to be developed. Thus, the total mass of the leg with the dummy mass was 16 kg. To prevent lateral motion, a passive three-DOF boom was attached to the hip center point, allowing free translation to the x- and z-axes and rotation to the y-axis of the thigh frame. Distance jumps that do not exploit the upper body mass and hip joints are challenging. However, as shown in Fig. 8(a) and (b), the leg performed a jump of 897 mm, which was the distance between the heel positions of the start and landing poses. Fig. 8(c), (d), and (e) show the motor and joint torques and the joint speed during jumping. The propulsion time was 0.32 s, and the aerial time between the takeoff and heel landing was 0.31 s. Fig. 8(c) shows that during the knee extension stage (0–0.15 s), the knee motor exerted a peak torque of 2.68 Nm, and the other three motors exerted approximately 1 Nm. Therefore, as shown in Fig. 8(d), the knee joint could exert 183 Nm by the CA, which is substantially higher than the maximum torque exerted only by the knee actuator, 75.04 Nm. In the foot push-off stage (0.15~0.32 s), the ankle and toe motors exerted a combined near-peak torque of 1.63 Nm. At the end of this stage, the leg was already moving at a high speed; thus, to accelerate further, the toe must push the ground at a higher speed than the moving leg. As shown in Fig. 8(e), the speed of the toe joint rapidly increases at the moment of toe-off, propelling the leg forward. Overall, the results show that the knee accelerates the heavy body first, and then the ankle and toe push the ground to increase speed at the last moment of jumping, which is similar to a human jump; however, the detailed motions were different. For instance, the initial angle of the ankle shown in Fig. 8(a) is difficult for humans; however, it is suitable for the proposed mechanism because it has a wide range of motion and an approximately linear torque transmission relationship. Landing control was not within the scope of this study; however, appropriate joint stiffness and damping values were set by joint-space impedance control to absorb the impact from the ground.

V. Conclusion

This paper presented a novel biomechanics-inspired leg mechanism called HyperLeg, which included a one-DOF knee, a two-DOF ankle, and a one-DOF toe joint. HyperLeg has light, yet robust mechanisms that are remotely actuated by motors in the thigh frame. The implemented leg weighed 8.16 kg, and the mass of the parts under the knee was only 4.2 kg. A unique transmission mechanism composed of high-payload timing belts and linkage mechanisms was designed to achieve high stiffness and strength while allowing for a wide range of motion. The distance jumping experiment was conducted using a 7.8 kg dummy mass, considering the addition of the hip and upper body, and the results showed effective and natural motions. In future studies, a biped robot with two 7-DOF legs and multiple-DOF dual arms will be developed. Three-DOF hip joints cooperatively actuated for dynamic and intricate motions are designed. Cooperative actuation can degrade torque-velocity performance in specific motions, such as the plantar flexion of ankle and the dorsiflexion of toe. Also, the toe joint can complicate control and balance. Therefore, a thorough study and experiments should be conducted to exploit the redundancy of the toe joint comparing with other humanoid legs, and mitigate the performance degradation. The ABS frames were replaced by 3-D printed metal parts to withstand multiple impacts and heavy loads. Control algorithms that harness the new features of the robot will be developed. The proposed robot is expected to bridge the gap between the current humanoid robots and highly dynamic, agile, quiet, and safe human bodies.

References

[1] D. A. Neumann, "*Kinesiology of the Musculoskeletal System: Foundations for Rehabilitation*," 3rd ed., Elsevier, 2016, pp. 595, 717.

[2] M. J. Coughlin, C. L. Saltzman, and R. A. Mann, *"Mann's Surgery of the Foot and Ankle,"* 9th ed., Elsevier, 2013, pp. 14.

[3] S. Chou, H. Cheng, J. Chen, Y. Ju, Y. Lin, and M. Wong, "The Role of the Great Toe in Balance Performance," *in Journal of Orthopaedic Research*, vol. 27, no.4, pp. 549–554, 2009.

[4] "ASIMO Technical Information." [Online]. Available: https://asimo.ho nda.com/Abstract -Technical- Information/

[5] J. Englsberger et al., "Overview of the torque-controlled humanoid robot TORO," *in IEEE-RAS International Conference on Humanoid Robots (Humanoids)*, Madrid, Spain, 2014, pp. 916–923.

[6] T. Jung, J. Lim, H. Bae, K. K. Lee, H. M. Joe, and J. H. Oh, "Development of the Humanoid Disaster Response Platform DRC-HUBO+," *in IEEE Transactions on Robotics*, vol. 34, no. 1, pp. 1–17, 2018.
[7] J. Kim et al., "Development of the lower limbs for a humanoid robot," *in 2012 IEEE/RSJ International Conference on Intelligent Robots and Systems*, Vilamoura-Algarve, Portugal, 2012, pp. 4000–4005.
[8] J. Kim et al., "Balancing control of a biped robot," *in 2012 IEEE International Conference on Systems, Man, and Cybernetics (SMC)*, Seoul, South Korea, 2012, pp. 2756–2761.
[9] N. G. Tsagarakis, D. Caldwell, F. Negrello, et al., "WALK-MAN: A High Performance Humanoid Platform for Realistic Environments," *in Journal of Field Robotics*, Vol. 34, no. 4, pp. 1225–1259, 2017.
[10] H. -J. Kang et al., "Realization of biped walking on uneven terrain by new foot mechanism capable of detecting ground surface," *IEEE International Conference on Robotics and Automation,* Anchorage, USA, 2010, pp. 5167-5172.*10*
[11] Abdolahnezhad, et al., "Online Bipedal Locomotion Adaptation for Stepping on Obstacles Using a Novel Foot Sensor," *IEEE-RAS 21st International Conference on Humanoid Robots (Humanoids)*, 2022, pp. 344-349.
[12] P. M. Wensing, A. Wang, S. Seok, D. Otten, J. Lang, and S. Kim, "Proprioceptive actuator design in the MIT cheetah: Impact mitigation and high-bandwidth physical interaction for dynamic legged robots," *in IEEE Transactions on Robotics*, vol. 33, no. 3, pp. 509–522, 2017.
[13] Y. H. Shin et al., "Design of KAIST HOUND, a Quadruped Robot Platform for Fast and Efficient Locomotion with Mixed-Integer Nonlinear Optimization of a Gear Train," *in 2022 International Conference on Robotics and Automation (ICRA)*, Philadelphia, PA, USA, 2022, pp. 6614–6620.
[14] Y. Sim and J. Ramos, "Tello Leg: The Study of Design Principles and Metrics for Dynamic Humanoid Robots," *in IEEE Robotics and Automation Letters (RAL)*, vol. 7, no. 4, pp. 9318-9325, 2022.
[15] D. Kim, S. J. Jorgensen, J. Lee, J. Ahn, J. Luo, L. Sentis, "Dynamic locomotion for passive-ankle biped robots and humanoids using whole-body locomotion control," *in The International Journal of Robotics Research (IJRR)*, vol. 39, no. 8, pp. 936–956, 2020.
[16] M. Chignoli, D. Kim, E. Stanger-Jones and S. Kim, "The MIT Humanoid Robot: Design, Motion Planning, and Control For Acrobatic Behaviors," *in 2020 IEEE-RAS 20th International Conference on Humanoid Robots (Humanoids)*, Munich, Germany, 2021, pp. 1–8.16
[17] A. Badri-Spröwitz et al., "BirdBot achieves energy-efficient gait with minimal control using avian-inspired leg clutching," *Science Robotics*, vol. 7, issue 64, 2022.
[18] Hurst et al., "Leg Configuration for Spring-Mass Legged locomotion," U.S. Patent. US10,189,519B2, filed May 27, 2016.
[19] B. R. P. Singh and R. Featherstone, "Mechanical Shock Propagation Reduction in Robot Legs," *in IEEE Robotics and Automation Letters (RAL)*, vol. 5, no. 2, pp. 1183–1190, 2020.
[20] Y. Ogura et al., "Human-like walking with knee stretched, heel-contact and toe-off motion by a humanoid robot," *in 2006 IEEE/RSJ International Conference on Intelligent Robots and Systems (IROS)*, Beijing, China, 2006, pp. 3976–3981.
[21] K. Hashimoto et al., "A study of function of foot's medial longitudinal arch using biped humanoid robot," *in 2010 IEEE/RSJ International Conference on Intelligent Robots and Systems (IROS)*, Taipei, Taiwan, 2010, pp. 2206–2211.
[22] T. Sato, S. Sakaino, and K. Ohnishi, "Trajectory planning and control for biped robot with toe and heel joints," *in 2010 11th IEEE International Workshop on Advanced Motion Control (AMC)*, Nagaoka, Japan, 2010, pp. 129–136.
[23] W. Choi, G. A. Medrano-Cerda, D. G. Caldwell, and N. G. Tsagarakis, "Design of a variable compliant humanoid foot with a new toe mechanism," *in 2016 IEEE International Conference on Robotics and Automation (ICRA)*, Stockholm, Sweden, 2016, pp. 642–647.
[24] K. Fruend, A. L. Shu, F. C. Loeffl and C. Ott, "A Guideline for Humanoid Leg Design with Oblique Axes for Bipedal Locomotion," *IEEE-RAS 21st International Conference on Humanoid Robots (Humanoids)*, Ginowan, Japan, 2022, pp. 60-66.
[25] "NASA human data" [Online]. Available: https://msis.jsc.nasa.gov/sections/section03.htm25
[26] W. Jang, D. Kum, Y. Choi, and Y. Kim, "Self-Contained 2-DOF Ankle-Foot Prosthesis with Low-Inertia Extremity for Agile Walking on Uneven Terrain," *in IEEE Robotics and Automation Letters (RAL)*, 2021, vol. 6, no.4, pp. 8134–8141.